ELSEVIER

Journal of Nuclear Materials 313–316 (2003) 738–742

journal of nuclear materials

www.elsevier.com/locate/jnucmat

Thermographic observation of the divertor target plates in the stellarators W7-AS and W7-X

D. Hildebrandt [a,*], F. Gadelmeier [b], P. Grigull [b], K. McCormick [b], D. Naujoks [a], D. Sünder [a], W7-AS Team [b]

[a] *Max-Planck-Institut für Plasmaphysik, Euratom Ass., Mohrenstrasse 41, D-10117 Berlin, Germany*
[b] *Max-Planck-Institut für Plasmaphysik, Euratom Ass., D-85748 Garching, Germany*

Received 27 May 2002; accepted 30 September 2002

Abstract

Thermography is applied on the stellarator W7-AS to monitor the thermal load of the recently installed divertor targets. A three dimensional numerical code was developed to evaluate power fluxes arriving at the targets from the measured temporal evolution of the surface temperature distribution. Values of the thermal conductivity of the used CFC-target material for all three directions are required for this evaluation and determined by observing the propagation of controlled heat pulses applied by an infrared laser. The evaluation of the thermographic measurements during plasma operation shows characteristic spatial and temporal features of the arrived heat fluxes. Significant features in high density regimes like plasma detachment from the divertor target plates or strongly enhanced localised plasma radiation (MARFE) has been observed by the installed infrared cameras. The implications of these observations for the thermographic system for W7-X are shortly addressed.

PACS: 52.70.Kz
Keywords: Stellarator; Thermography; Island divertor; Heat deposition; Divertor detachment; MARFE

1. Introduction

The stellarator W7-AS has recently been equipped with ten open divertor modules in order to experimentally examine the island divertor concept considered for the W7-X device presently under construction [1]. The installed divertor allows now access to a new very high density (up to $n_e = 4 \times 10^{20}$ m^{-3}) operating regime under quasi-stationary condition with improved confinement properties and substantial reduction of power fluxes to the targets [2]. The plasma target interaction has been diagnosed by two infrared cameras observing an upper and a lower target. In Section 2 some experimental details of the divertor components and the thermographic system are described. The evaluation procedure to derive the power fluxes arriving at the target plates from the thermographic measurements is given in Section 3. In order to determine the heat conductivity of the CFC divertor target material needed for this evaluation accompanying experiments with target power loading experiments by heat pulses of laser radiation have been done. These results are shown in Section 4. Section 5 demonstrates a comparison of thermographic and calorimetric measurements on the target plates. Significant features of the thermographic measurements in high density regimes like plasma detachment from the divertor target plates or strongly enhanced localized plasma radiation (MARFE) are shown in Section 6. Finally, the proposed thermographic

* Corresponding author. Tel.: +49-30 203 66 101; fax: +49-30 203 66 111.
E-mail address: hildebrandt@ipp.mpg.de (D. Hildebrandt).

0022-3115/03/$ - see front matter
PII: S0022-3115(02)01490-3

system for supervising and diagnosing the divertor target load of the stellarator W7-X presently under construction is sketched out in Section 7.

2. Experimental details

W7-AS is a modular stellarator with five magnetic field periods. The major and minor radii are $R = 2$ m and $a < 0.16$ m, respectively. The magnetic field strength at the axis is $B < 2.5$ T. Heating of the high density plasma is accessible via NBI with a power up to 2.5 MW.

The plasma cross section per period varies from elliptical to triangular and back to elliptical. At high rotational transform ($\iota = 5/9$) macroscopic magnetic islands occur at the plasma boundary. Their size and position can be adjusted. The divertor consists of ten identical modules placed at the top and bottom of the elliptical cross section. Each module consists of an inertially cooled target of CFC-material which intersects the islands, and of baffles (fine grained graphite-EK 98). The targets are three-dimensionally shaped by 17 thermally insulated tiles (thickness between 20 and 30 mm) in order to achieve nearly homogeneous thermal load distribution in the helical direction. Many of the target tiles are equipped with thermocouples located near the centre of the tiles and 5 mm behind its plasma-facing surface. The thermocouples measure the tile temperature trace before the discharge and during a time period of about 30 s starting 5 s after the discharge. Two IR-cameras operating in the wavelength region from 3 to 5 μm are installed to measure the surface temperature of the lower target tiles in module 1 and the upper tiles of module 2 during the discharge. The spatial resolution given by the infrared optics is 2 and 4 mm, respectively. Measurements have been done with frame rates of 315 and 50 Hz. Thermography systems are also used on JET, ASDEX-Upgrade, Tore Supra and TEXTOR-94 [3–5].

3. Modelling

The power flux to the target is derived from the temporal evolution of the measured surface temperature distribution by solving the non-stationary heat conduction equation inside the target tiles.

$$\frac{\partial T}{\partial t} = \left(a_x \frac{\partial^2 T}{\partial x^2} + a_y \frac{\partial^2 T}{\partial y^2} + a_z \frac{\partial^2 T}{\partial z^2} \right)$$
$$\text{with } a_i = \frac{\lambda_i}{c_p \rho} \text{ and } i = x, y, z. \quad (1)$$

Here a_i, λ_i, c_p and ρ are the heat diffusion coefficients, the heat conductivities, the specific heat capacity and the density, respectively.

The results are obtained by means of the finite difference method in a three dimensional (3D) geometry.

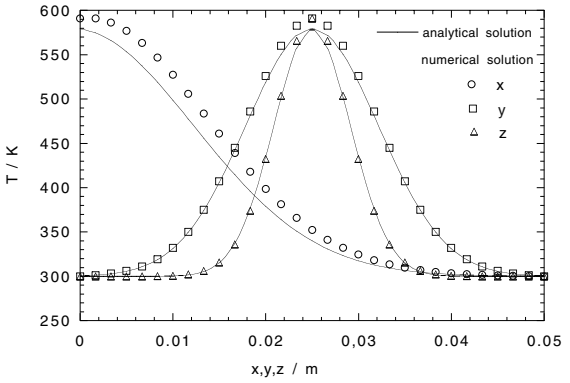

Fig. 1. Spatial temperature distribution at $t = 1$ s after a local and sudden heat flux of $Q = 2000$ J as calculated with the numerical code in comparison with the analytical results with different heat conduction coefficients for the x-, y-, z-directions where x is the direction into the target. λ_x, λ_y, λ_z are assumed to be 200, 60 and 20 W/m K, respectively.

The calculation is done for each target tile separately. A number of 120 000 grid points have been chosen corresponding to a spatial step width between 0.1 and 4 mm. The time step for the calculation was 2 ms. Neumann boundary conditions (given temperature gradient) are applied. The unloaded surface areas of the tiles are treated as thermally insulated.

In order to validate the results of the numerical technique a comparison with the analytical solution of the non-stationary heat conduction equation for a local and sudden heat pulse $Q = Q_0 \delta(x)\delta(y - y_0)\delta(z - z_0)\delta(t)$ at the surface of a semi-infinite target ($0 \leqslant x \leqslant \infty$) was made.

The analytical solution of Eq. (1) is then given by [6]:

$$T(x, y, z, t) = \frac{2Q_0}{c_p \rho (4\pi t)^{3/2} \sqrt{a_x a_y a_z}} \times \exp - \left[\frac{x^2}{4a_x t} + \frac{(y - y_0)^2}{4a_y t} + \frac{(z - z_0)^2}{4a_z t} \right]. \quad (2)$$

Fig. 1 shows a good agreement between the analytical and numerical results if appropriate time and spatial steps are chosen (see above).

4. Heat conductivity of CFC

In order to determine the heat conductivity for the used CFC-target material the temporal evolution of the temperature distribution at the surface of a target tile was measured after applying heat pulses by an infrared laser and has been compared with the analytical solution of the 3D heat conduction equation. Both, the power and the duration of the laser pulse, can be varied.

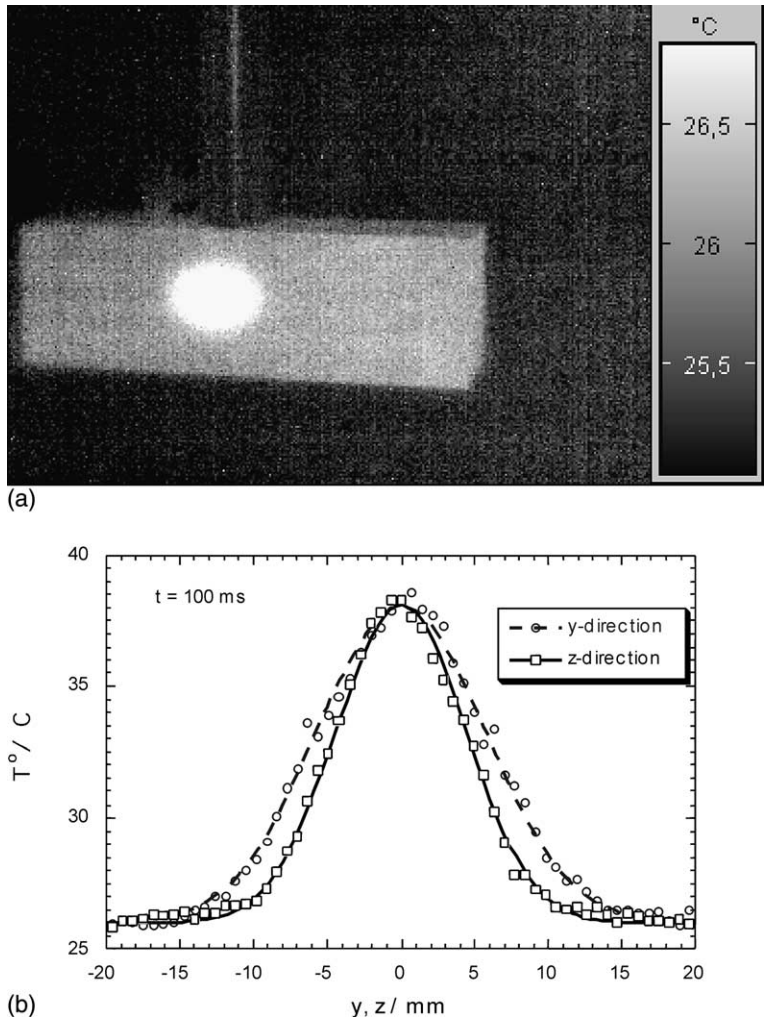

Fig. 2. (a) Thermographic image of a CFC-target tile taken 100 ms after a 20 J heat pulse by an infrared laser with a light diameter of about 3 mm. The spot has an extension of about 20 mm in this picture. (b) Temperature distribution in the horizontal y- and vertical z-direction extracted from the data of Fig. 2(a). The curves are the results of the analytic solution (Eq. (2)) with the fitted parameter $\lambda_{x,y} = 220$ W/m K and $\lambda_z = 130$ W/m K, respectively.

Fig. 2(a) shows an IR-image of the tile surface 100 ms after application of a circular laser energy pulse ($\lambda = 1.06$ mm) of 20 J with a diameter of 3 mm and a duration of 20 ms. The image sequence showed clearly the anisotropic heat propagation of this material. Note the elliptical shape of the temperature distribution in Fig. 2(a) taken 100 ms after the pulse. In Fig. 2(b) the lateral distribution of the surface temperature for different directions derived from Fig. 1(a) is plotted and compared with calculated results obtained by the analytical solution (2) with fitted values for the thermal conductivity. The derived values of this conductivity at room temperature are $\lambda_{x,y} = 220$ W/m K and $\lambda_z = 130$ W/m K, respectively. The corresponding values reported by the manufacturer are $\lambda_{x,y} = 220$ W/m K and $\lambda_z = 180$ W/m K, respectively.

5. Comparison of thermography and calorimetry

The temporal evolution of both, the bulk temperature measured by the thermocouples and the surface temperature at the position of the thermocouple measured by thermography were compared. Fig. 3(a) displays the temporal traces of the bulk temperature of a target tile (tile 10) measured by the installed thermocouple before and after two discharges with a similar magnetic configuration (values during the discharge

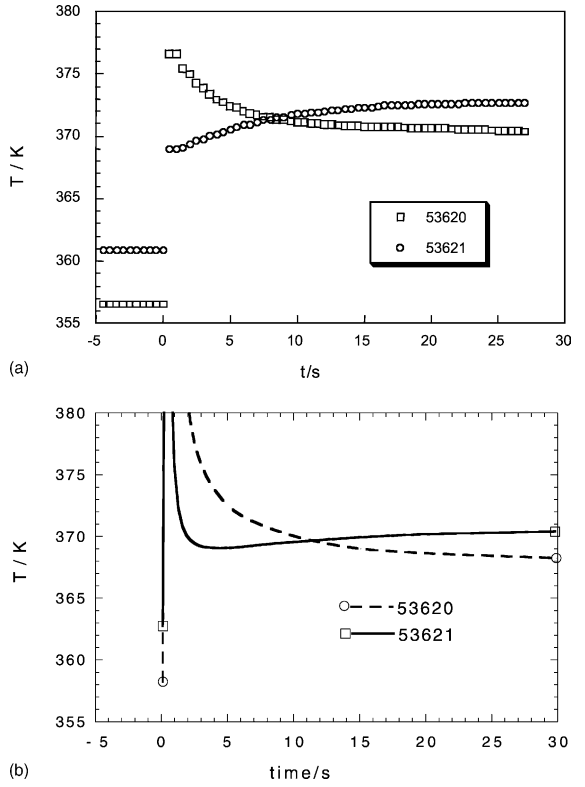

Fig. 3. Temporal evolution of the bulk temperature of a target tile measured by a thermocouple (a) and of the surface temperature measured by thermography (b) for two discharges with different plasma density.

could not be evaluated). Remarkable is the different temporal evolution of the measured temperature after the discharge. The discharges were performed with an absorbed NBI-power of 2.5 MW and a slightly different plasma density, $n_e = 2.2 \times 10^{20}$ m^{-3} (shot 53620) and $n_e = 2.5 \times 10^{20}$ m^{-3} (shot 53621). These values are just below and above the observed threshold density for transition from normal confinement to improved confinement of the high density H-mode [7]. Attended to improved confinement is a change of the n_e-profile and the heat flux deposition pattern at the targets. The variation of the deposition pattern causes the different temporal evolution of the tile temperature at the position of the thermocouple seen in Fig. 3(a). This is confirmed by the 2D-thermographic image data that show temporal evolutions of the surface temperature at this position for both discharges quite similar to that measured by the thermocouple (compare Fig. 3(a) and (b)) and can be explained by the heat propagation in the material.

Values of the deposited energy on the target tiles derived from both methods differ by about 30% in this case. Generally, the deviations in the deposited energy derived from both methods agree within a factor of 2.

6. Thermographic features at target plates of W7-AS

The evaluation of the thermographic measurements during plasma operation shows typical spatial and temporal features of the heat fluxes arrived at the target plates. The observed heat deposition pattern can be quite well correlated to the magnetic configuration. In the favourable divertor configuration with macroscopic magnetic islands at the plasma edge (rotational transform $\iota \approx 5/9$) the observed poloidal heat flux diversion agrees well with the Hα-emission pattern and the expected target-island intersection lines [7]. Due to the island structure, the main interaction of the plasma with the targets concentrates at two helical stripes seen in Fig. 4. Dark zones within the stripes mark the edges of the target tiles.

The temporal evolution of the target surface temperature reflects typical plasma phenomena. In fact, partial plasma detachment from the targets indicated by a strong reduction of the derived power fluxes at the targets up to a factor of 10 was observed for plasma densities higher than 2.5×10^{20} m^{-3}. The transition from attached to partially detached states could be continuously performed in a controlled way by a linearly

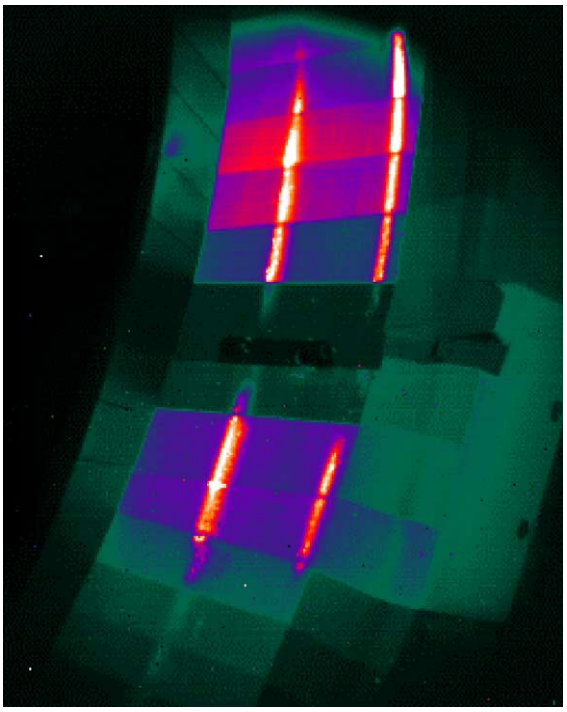

Fig. 4. Typical heat deposition pattern at the target for discharges with the rotational transform $\iota = 5/9$ showing two helical stripes of heat load at the target. Each target tile of the upper target is visible. Two central target tiles are less loaded because their radial position is some mm behind the others.

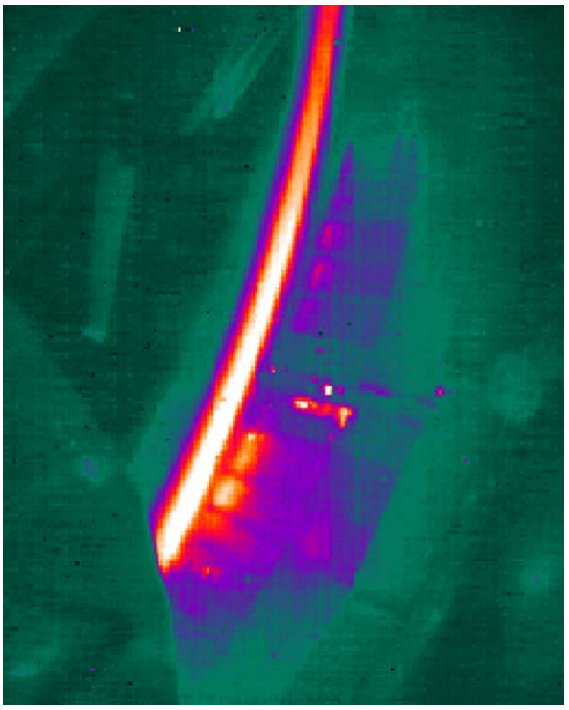

Fig. 5. Thermographic image showing a MARFE in front of the upper target in module 2.

ramped plasma density. With increasing density the radiated power fraction from the plasma boundary grows smoothly and leads to the onset of plasma detachment at the target plates. The detachment is always partial; the plasma at a certain small target region, far from the main plasma but with steeper inclination to the field lines stays attached even at highest densities. With increasing detachment, the up/down parameters at the targets become increasingly asymmetric. Moreover, the radiation from the separatrix region becomes asymmetric, indicating a MARFE-like development. At highest plasma densities very intensive MARFEs can be observed by the infrared cameras in front of the upper or lower targets depending on the magnetic field direction as a bright continuous stripe (see Fig. 5) in contrast to the discontinuous stripe of the radiation from the target. The MARFE-region follows the toroidal direction but the radiated power density varies along this direction. The radial extension at the toroidal position with highest radiated power density is about 3 cm. The MARFE appears for a time period of about 5 ms. The limited lifetime is due to the control of the plasma density via Bremsstrahlung. A strong increase of this signal at the appearance of the MARFE caused immediate closing of the gas inlet valves and a decrease of the plasma density. It is obvious that due to the high level of radiation from the plasma the surface temperature of the target and hence the power flux to the targets can not be inferred at the appearance of MARFEs.

7. Thermographic system of W7-X

The successive device W7-X presently under construction will be equipped with island divertor modules similar to that of W7-AS but they have much larger dimensions (5 m toroidal extension for W7-X compared to about 1 m for W7-AS). To guarantee the safety of the divertor and to monitor its operation mode thermography with data evaluation in real time is considered besides other diagnostics. To be able to determine local power deposition, to detect asymmetries of heat load to the targets and to prevent damage of target elements by overheating or mechanical defects a continuous supervision of the target surface area is essential. For the thermography system ten uncooled microbolometer cameras operating in the wavelength region from $\lambda = 8$ to 15 μm will be installed. This seems to be of advantage, in particular, for very high-density regimes. Disturbing plasma radiation in this wavelength region is expected to be lower than that in the wavelength region from 3 to 5 μm observed in the present experiment (e.g. Bremsstrahlung-intensity scales with λ^{-2}).

References

[1] P. Grigull et al., Plasma Phys. Contr. Fusion 43 (2001) A175.
[2] K. McCormick et al., Phys. Rev. Lett. 89 (2002) 0150001.
[3] A. Herrmann, these Proceedings.
[4] R. Reichle et al., J. Nucl. Mater. 290–293 (2001) 701.
[5] K.H. Finken et al., J. Nucl. Mater. 290–293 (2001) 1064.
[6] D. Sünder, private communication.
[7] K. McCormick et al., these Proceedings.